NATIONAL TECHNICAL UNIVERSITY OF ATHENS

SCHOOL OF APPLIED MATHEMATICS AND PHYSICAL SCIENCES

"Microsystems and Nanodevices"

Interdepartmental Program of Graduate Studies

Thermodynamic Analysis of *n*-Hexane/Ethanol Binary Mixtures Using Kirkwood-Buff Theory

Master's thesis of

Panagiotis Petris

Supervisor

Doros N. Theodorou

Professor, School of Chemical Engineering, NTUA

Athens

June 2018

Acknowledgments

The subject of this thesis, as well as the fundamental guidelines on combining existing theoretical works and methodologies, were suggested by professor Doros Theodorou. His high standards, along with his valuable insight on any matter raised in the course of this thesis, were decisive for the quality of this work.

I am particularly grateful to Dr. Stefanos Anogiannakis for providing me with the very much needed theoretical and computational background, as well as for his endless willingness to help me with any issue that came up, in this one year of my collaboration with him. I am also grateful to Ph.D. candidate Panagiotis-Nikolaos Tzounis for sharing his knowledge with me, and for his immense help on critical points of this thesis. I have, also, been helped and educated by interacting with Ph.D. candidate Vasilis Georgilas, as well as all the members of COMSE group. I have to thank my committee members Leonidas Tsetseris and Epaminondas Voutsas for devoting their time to assessing this thesis.

The research leading to these results has received funding from the European Union Seventh Framework Programme (FP7/2007–2013) under grant agreement no. 619793 CoLiSA.MMP. Scienomics SARL is gratefully acknowledged for making their software available to us through the Scienomics Group of Scientific Excellence (SGSE) program.

Contents

Acknowledgments 3
List of Symbols 6
List of Figures 14
List of Tables 15
Abstract 16
1. Thermodynamics of Mixing 17
1.1 Kirkwood-Buff Theory 17
1.2 Mixing properties 21
1.2.1 Perfect gases 22
1.2.2 Ideal solutions 23
1.2.3 Real mixtures 27
1.3 Gibbs energy, enthalpy and entropy of mixing 28
1.4 Excess properties 29
2. Atomistic simulations 31
2.1 Introduction 31
2.2 Molecular Dynamics algorithm 33
2.3 Computer Clusters 35
3. Systems studied 36
3.1 Simulation details 36
3.2 Force Field 38
4. Methodology 41
4.1 Extension to Isobaric-Isothermal Ensemble 41
4.2 Molecule and segment based methods 43
5. Results and Discussion 46
5.1 Density 46
5.2 Pair distribution functions 47
5.3 Kirkwood-Buff integrals 49
5.4 Activity Coefficients 51
5.5 Excess Gibbs Energy, excess enthalpy, and excess entropy 54
Conclusions 60

Future Work 62
Appendix 1 63
Appendix 2 64
Bibliography 66

List of Symbols

A^E	Excess Helmholtz energy
A_{ij}	Chemical potential derivative divided by temperature and Boltzmann's constant
$\lvert A\rvert_{ij}$	Co-factor of A_{ij}
A_n	Constant of dihedral potential
$\lvert A\rvert$	Determinant of matrix with elements A_{ij}
f	Fugacity
f_i	Fugacity of component *i*
f_i^0	Fugacity of component *i* in a reference state

f_i^V	Fugacity of component *i* in vapor phase
f_i^L	Fugacity of component *i* in liquid phase
$f_i^{V,pure}$	Fugacity of pure component *i* in vapor phase
$f_i^{L,pure}$	Fugacity of pure component *i* in liquid phase
$g_{ij}^{\mu VT}$	Pair distribution function defined in the open grand canonical ensemble for two species *i* and *j*
g_{ij}, g_{ij}^{NpT}	Pair distribution function defined in the *NpT* ensemble for two species *i* and *j*
G	Gibbs energy per molecule
$G_{ij}^{\mu VT}$	Kirkwood-Buff (KB) integrals in the grand canonical ensemble μVT
G_{ij}, G_{ij}^{NpT}	Kirkwood-Buff (KB) integrals in the *NpT* ensemble
G_{ij}^{∞}	limiting value of KB integrals for $V \to \infty$

G^{E}	Excess Gibbs energy
$G_{\mathrm{m}}^{\mathrm{E}}$	Molar excess Gibbs energy
h	Step in the mole fraction used while applying the shooting method for the integration of the second derivative of Gibbs free energy
H	Enthalpy per molecule
H^{mixture}	Enthalpy of the mixture
H_i^{pure}	Enthalpy of pure component i
H^{E}	Excess enthalpy
$H_{\mathrm{m}}^{\mathrm{E}}$	Molar excess enthalpy
$\mathcal{H}_{N_1 \ldots N_\nu}$	Hamiltonian for system of molecules $N_1 \ldots N_\nu$
k_{B}	Boltzmann constant
k_{b}	Harmonic oscillator constant

k_θ	Harmonic oscillator constant
l_{cell}	Edge length of each cell of the simulation box after partitioning in order to calculate KB integrals
l	Bond length
l_0	Bond length in equilibrium state
N	Number of molecules in mixture
N_{A}	Avogadro's number
N_i	Number of molecules of species *i*
$\langle N_i \rangle$	Average number of molecules of species *i*
N_{cells}	Number of cells constructed within simulation box
p	Pressure
p_i^s	Saturated pressure of component *i*

P	Probability density function on μVT
$\mathbf{r}_1, \mathbf{r}_2$	Positions on volume V
S^{E}	excess entropy
$S_{\mathrm{m}}^{\mathrm{E}}$	molar excess entropy
T	Temperature
$\mathcal{V}_{\mathrm{LJ}}$	Lennard-Jones (6,12) potential energy
$\mathcal{V}_{\mathrm{bonded}}$	Dynamic energy of intermolecular interactions
$\mathcal{V}_{\mathrm{non\text{-}bonded}}$	Dynamic energy of intramolecular interactions
$\mathcal{V}_{\mathrm{bond}}$	Bond stretching potential
$\mathcal{V}_{\mathrm{bend}}$	Angle bending potential
$\mathcal{V}_{\mathrm{torsion}}$	Torsional angle potential

$\mathcal{V}_{\text{Coul}}$	Coulomb potential
$\mathcal{V}$	Potential energy of system
U	Internal energy
$v_i^{(1)}(\mathbf{r}_1)$	Density of component *i* at position $\mathbf{r}_1$
$v_{ij}^{(2)}(\mathbf{r}_1, \mathbf{r}_2)$	Density of ordered molecule couples of type *i* and *j*, where molecule type 1 is at position $\mathbf{r}_1$ and molecule type 2 is at position $\mathbf{r}_2$
V_0	Minimum volume of the simulation box during an *NpT* simulation
$\langle V \rangle$	Average volume in *NpT* simulation
a_{ij}	Constant which depends only on intensive thermodynamic system such as density and temperature
γ_i	Activity coefficient of component *i*
δ_{ij}	Kronecker delta
$\Delta_{\text{mix}} G$	Gibbs energy of mixing

$\Delta_{\mathrm{mix}} G^{\mathrm{id}}$	Gibbs energy of mixing for ideal solutions
$\Delta_{\mathrm{mix}} G_{\mathrm{m}}$	Molar Gibbs energy of mixing
$\Delta_{\mathrm{mix}} H$	Enthalpy of mixing
$\Delta_{\mathrm{mix}} H^{\mathrm{id}}$	Enthalpy of mixing for ideal solutions
$\Delta_{\mathrm{mix}} H_{\mathrm{m}}$	Molar enthalpy of mixing
$\Delta_{\mathrm{mix}} S$	Entropy of mixing
$\Delta_{\mathrm{mix}} S^{\mathrm{id}}$	Entropy of mixing for ideal solutions
$\Delta_{\mathrm{mix}} S_{\mathrm{m}}$	Molar entropy of mixing
ε_{ij}	Depth of the Lennard-Jones potential well
θ	Bond angle
θ_0	Bond angle in equilibrium state

κ_T	Isothermal compressibility
λ	Parameter which indicates the fineness of partitioning of the simulation box
μ_i	Chemical potential of component *i* per molecule
ρ	Total number density (molecules per unit volume, all species)
ρ_{mass}	Mass density
ρ_i	Number density of species *i*
$\rho_i^{(1)}(\mathbf{r}_1)$	Average number density of component *i* at position $\mathbf{r}_1$
$\rho_{ij}^{(2)}(\mathbf{r}_1,\mathbf{r}_2)$	Average number density of ordered molecule couples of type *i* and *j*, where molecule type 1 is at position $\mathbf{r}_1$ and molecule type 2 is at position $\mathbf{r}_2$
φ	Torsional angle between two planes
Ω	Grand partition function (μVT ensemble), equal to $-pV$ in an isotropic system.

List of Figures

Figure 1: Pressure-composition diagrams for the binary mixtures of *n*-hexane/ethanol at *T*=298.15 K as determined from experimental data [11] (top), and at *T*=413.15 K as determined from simulation results [9] and experimental data [10] (bottom)…. ..36

Figure 2: Bonded interactions of (a) bond, (b) angle, and (c) dihedral angle 38

Figure 3: Snapshot of equimolar *n*-hexane/ethanol binary mixture at $T = 298.15\text{K},\ p = 1\text{atm}$ (a), as well as at $T = 413.15\text{K},\ p = 20\text{atm}$ (b). Cyan molecules represent *n*-hexane, while red molecules represent ethanol.. 41

Figure 4: Schematic presentation of molecule based method and segment based method, used for calculating fluctuations in the numbers of particles 43

Figure 5: Plot of λG_{11}, λG_{22}, λG_{12} versus λ for the equimolar n-hexane/ethanol binary mixture at $T = 298.15\text{K},\ p = 1\text{atm}$ (a), as well as at $T = 413.15\text{K},\ p = 20\text{atm}$ (b), for both molecule and segment based methods……..44

Figure 6: Molecular density of mixtures versus mole fraction of n-hexane for the n-hexane/ethanol binary mixture, simulated with 1,000 and 10,000 molecules at $T = 298.15\text{K},\ p = 1\text{atm},$ and at $T = 413.15\text{K},\ p = 20\text{atm},$ compared to experimental data at $T = 298.15\text{K},\ p = 1\text{atm}$ [15] 46

Figure 7: Pair distribution functions for equimolar *n*-hexane/ethanol binary mixture versus distance *r,* at both $T = 298.15\text{K},\ p = 1\text{atm},$ and $T = 413.15\text{K},\ p = 20\text{atm}$ 47

Figure 8: KB integrals calculated from both pair distribution functions and particle fluctuations, for *n*-hexane/ethanol binary mixtures with *n*-hexane mole fractions equal to $x_1 = 0.1, 0.5, 0.9,$ at *T*=413.15 K, *p*=20 atm 49

Figure 9: Activity coefficients γ_1, γ_2 plotted versus *n*-hexane mole fraction, x_1, for *n*-hexane/ethanol binary mixtures, as calculated from molecule and segment based methods, being compared to experimental data at *T*=298.15 K, *p*=1 atm [11] (a), (b). Activity coefficients γ_1, γ_2 plotted and compared to Chen's simulation [9] and experimental data [10] at *T*=413.15 K, *p*=20 atm (c), (d) 51

Figure 10: Molar excess Gibbs energy plotted versus *n*-hexane mole fraction, x_1, for *n*-hexane/ethanol binary mixtures, as calculated from molecule and segment based methods, using the activity coefficients method (a) and the iterative shooting method (b). Calculations are compared to experimental data at *T*=298.15 K, *p*=1 atm [11]. Molar excess Gibbs energy as calculated using the activity coefficients method (c) and the iterative shooting method (d), being compared to Chen's simulation [9] and experimental data [10] at *T*=413.15 K, *p*=20 atm..... 54

Figure 11: Excess molar Gibbs energy, excess molar enthalpy, and excess molar entropy plotted versus *n*-hexane mole fraction, x_1, for *n*-hexane/ethanol binary mixtures, being compared to experimental data at T=298.15 K, p=1 atm [11] (top). Excess molar Gibbs energy, excess molar enthalpy, and excess molar entropy plotted and compared to Chen's simulation [9] and experimental data at T=413.15 K, p=20 atm [10] (bottom). 55

Figure 12: Flow diagram of the iterative shooting method we apply to solve equation (5.1) numerically 61

List of Tables

Table 1: Lennard – Jones potential parameters of TraPPE-UA for *n*-hexane 59

Table 2: Lennard – Jones potential parameters of TraPPE-UA for ethanol 59

Table 3: Bonded interactions parameters……60

Abstract

A complete thermodynamic analysis of mixtures consisting of molecules with complex chemical constitution can be a rather rigorous process. Kirkwood-Buff theory of solutions allows the estimation of thermodynamic properties which cannot be directly extracted from atomistic simulations, such as the Gibbs energy of mixing ($\Delta_{mix}G$). In this work, we perform molecular dynamics simulations of *n*-hexane/ethanol binary mixtures in the liquid state under two temperature-pressure conditions and at various mole fractions. Based on the recently published methodology of Galata et al. (A.A. Galata, S.D. Anogiannakis, D.N. Theodorou, Thermodynamic Analysis of Lennard-Jones binary mixtures using Kirkwood-Buff theory, Fluid Phase Equilib. 470 (2018) 25-27), we first calculate the Kirkwood-Buff (KB) integrals in the isothermal-isobaric, *NpT*, ensemble, identifing how system size affects their accurate estimation of KB. We, then, extract the activity coefficients, excess Gibbs energy, excess enthalpy, and excess entropy for the *n*-hexane/ethanol binary mixtures we simulate. We employ two approaches for quantifying composition fluctuations: one based on counting molecular centers of mass, and a second one based on counting molecular segments. Results from the two approaches are practically indistinguishable. We compare our results against the predictions from vapor-liquid equilibria obtained in a previous simulation work using force field, as well as with experimental data, and find very good agreement.

Key Words: Kirkwood-Buff Theory, *n*-hexane/ethanol mixture, excess properties, pair distribution functions, activity coefficients

Chapter 1

1. Thermodynamics of Mixing

1.1 Kirkwood-Buff Theory

Kirkwood Buff (KB) theory (1951)[1] is the most important theory of solutions. It was developed originally in the grand canonical ensemble. The key advantage is that through the calculation of the well-known KB integrals, one can derive thermodynamic properties. These KB integrals can be calculated from the above relation in the μVT ensemble

$$G_{ij}^{\mu VT} = \int_0^\infty [g_{ij}^{\mu VT}(r) - 1] 4\pi r^2 dr \quad (1.1)$$

where $g_{ij}^{\mu VT}(r)$ is the pair distribution function defined in the open grand-canonical ensemble for two species *i* and *j* and r is the Euclidean distance between molecules of these two species. Thus, the theory may be used to compute thermodynamic quantities based on our knowledge of the pair distribution function. Symbolically

$$\{G_{ij}\} \rightarrow \{\kappa_T, \partial\mu_i / \partial x_i, ...\}$$

An alternative definition of KB integrals is based on particle number fluctuations inside a reference volume V in the grand canonical ensemble. [2] To establish that definition, an open region of volume V is considered. That region is a part of an infinite size system. In the μVT representation selected, at a certain time instant, let volume V contain exactly N_1, N_2, ..., N_ν molecules of the ν molecular species constituting the multi-component system. In this representations of molecules in space, the density of molecule type i in position $\mathbf{r}_1$, $v_i^{(1)}(\mathbf{r}_1)$, as well as density of ordered pair of molecules of type i and j, $v_{ij}^{(2)}(\mathbf{r}_1,\mathbf{r}_2)$ (where molecule 1 is positioned on $\mathbf{r}_1$ and molecule type 2 is positioned on $\mathbf{r}_2$) is calculated from the following relations

$$v_i^{(1)}(\mathbf{r}_1)=\sum_{k_i=1}^{N_i}\delta(\mathbf{r}_{k_i}-\mathbf{r}_1) \quad (1.2)$$

$$v_{ij}^{(1)}(\mathbf{r}_1,\mathbf{r}_2)=\sum_{k_i=1}^{N_i}\sum_{l_j=1}^{N_j}\delta(\mathbf{r}_{k_i}-\mathbf{r}_1)\delta(\mathbf{r}_{l_j}-\mathbf{r}_2) \quad \text{for } k_i\neq l_j \quad (1.3)$$

where $\delta(\mathbf{r}_{k_i}-\mathbf{r}_1)$ is the three-dimensional Dirac delta function. Upon integration, these densities satisfy the following relations:

$$\int_V v_i^{(1)}(\mathbf{r}_1)dV_1=N_i \quad (1.4)$$

$$\int_V\int_V v_{ij}^{(2)}(\mathbf{r}_1,\mathbf{r}_2)dV_1dV_2=N_iN_j-N_i\delta_{ij} \quad (1.5)$$

where δ_{ij} is Kronecker delta, which is equal to one for $i=j$ and zero for $i\neq j$. The corresponding ensemble averaged number densities $\rho_i^{(1)}(\mathbf{r}_1)$ and $\rho_{ij}^{(2)}(\mathbf{r}_1,\mathbf{r}_2)$ are calculated as

$$\rho_i^{(1)}(\mathbf{r}_1) = \left\langle v_i^{(1)} \right\rangle \quad (1.6)$$

$$\rho_{ij}^{(2)}(\mathbf{r}_1, \mathbf{r}_2) = \left\langle v_{ij}^{(2)} \right\rangle \quad (1.7)$$

These densities are calculated for all N_1, N_2, ..., N_ν, and for the whole phase space, for every group of atoms, according to the probability density function, P, in the grand canonical (μVT) emsembl, which is

$$P = \exp\left[\frac{\Omega + \sum_{i=1}^{\nu} N_i \mu_i - \mathcal{H}_{N_1 \ldots N_\nu}}{k_B T} \right] \quad (1.8)$$

where μ_i is the chemical potential of type i per molecule, $\mathcal{H}_{N_1 \ldots N_\nu}$ the Hamiltonian of a group of molecules $N_1 \ldots N_\nu$, k_B is Boltzmann's constant, and Ω is the grand potential. In the distribution of equation (1.8), the grand partition function $\Xi = \exp[-\Omega/(k_B T)]$ plays the role of a normalizing constant. In a homogeneous system, Ω equals. The calculations of mean values of equations (1.6) and (1.7) generate the following relations for the integrals of average densities

$$\int_V \rho_i^{(1)}(\mathbf{r}_1) dV_1 = \left\langle N_i \right\rangle \quad (1.9)$$

$$\int_V \int_V \rho_{ij}^{(2)}(\mathbf{r}_1, \mathbf{r}_2) dV_1 dV_2 = \left\langle N_i N_j \right\rangle - \delta_{ij} \left\langle N_i \right\rangle \quad (1.10)$$

$$\int_V \int_V \left[\rho_{ij}^{(2)}(\mathbf{r}_1, \mathbf{r}_2) - \rho_i^{(1)}(\mathbf{r}_1) \rho_j^{(1)}(\mathbf{r}_2) \right] dV_1 dV_2 = \left[\left\langle N_i N_j \right\rangle - \left\langle N_i \right\rangle \left\langle N_j \right\rangle \right] - \delta_{ij} \left\langle N_i \right\rangle \quad (1.11)$$

For a fluid system, such as a liquid solution or a mixture of gases, average densities are obtained as

$$\rho_i^{(1)}(\mathbf{r}_1) = \frac{\langle N_i \rangle}{V} \quad (1.12)$$

$$\rho_{ij}^{(2)}(\mathbf{r}_1, \mathbf{r}_2) = \frac{\langle N_i \rangle}{V} \frac{\langle N_j \rangle}{V} g_{ij}^{(2)}(r) \quad (1.13)$$

$$r = |\, \mathbf{r}_2 - \mathbf{r}_1 \,| \quad (1.14)$$

where $g_{ij}^{(2)}(r)$ is the pair distribution function between molecules of type *i* and *j*, which depends exclusively on the distance *r* of pair *ij*. Combining equations (1.9) - (1.14) we obtain

$$\int [g_{ij}^{(2)}(r) - 1] dV = V \left(\frac{\langle N_i N_j \rangle - \langle N_i \rangle \langle N_j \rangle}{\langle N_i \rangle \langle N_j \rangle} - \frac{\delta_{ij}}{\langle N_i \rangle} \right) \quad (1.15)$$

where integral is extended on any relative coordinates of pair *i* and *j*.

Any observed variations on the composition of a thermodynamically open system, of volume *V*, is directly correlated to thermodynamic parameters via the relations

$$\langle N_i N_j \rangle - \langle N_i \rangle \langle N_j \rangle = \frac{|A|_{ij}}{|A|} \quad (1.16)$$

$$|A| = |A_{ij}| \quad (1.17)$$

$$A_{ij} = \frac{1}{k_B T} \left(\frac{\partial \mu_i}{\partial N_j} \right)_{T,V,N_{k \neq j}} \quad (1.18)$$

where $|A|_{ij}$ is the co-factor of A_{ij} in the determinant $|A|$ of the matrix with elements A_{ij}, μ_i is the chemical potential per molecules of type *i*, and *T* is the system temperature. Combining above relations leads to the final relation between the Kirkwood-Buff integral and the covariance in the numbers of particles within volume *V*.

$$G_{ij}^{\mu VT} = \int [g_{ij}^{(2)}(r) - 1] dV = V \left(\frac{\langle N_i N_j \rangle - \langle N_i \rangle \langle N_j \rangle}{\langle N_i \rangle \langle N_j \rangle} - \frac{\delta_{ij}}{\langle N_i \rangle} \right) \quad (1.19)$$

KB theory of solutions was initially developed to obtain thermodynamic properties from pair distribution functions. In most cases, pair distribution functions are not easily extracted either from analytical calculations, or from computer simulations. The inversion of KB theory was developed from Ben-Naim (1977),[3] and it provided a methodology on calculating KB integrals from thermodynamic quantities. Symbolically the inversion theory may be written as

$$\{\kappa_T, \partial \mu_i / \partial x_i, ...\} \rightarrow \{G_{ij}\}$$

where the quantities G_{ij} can be extracted from measurable thermodynamic quantities. In a strict sense, G_{ij} are not molecular properties. However, they do convey information on the local mode of packing of various species. As such, the theory provides a powerful tool to probe local properties of the mixtures. Ever since the publication of the inversion of the KB theory, the number of papers published on subjects related to the theory has grown steadily and dramatically.

1.2 Mixing properties

The thermodynamic properties of any pure substance are dictated by the intermolecular forces developed between the molecules of this substance. The same applies for the thermodynamic

properties of a mixture, but on a mixture, one has to calculate forces between molecules belonging to different components as well.

1.2.1 Perfect gases

In his attempt at simplifying the concept of chemical potential, G. N. Lewis initially considered chemical potential for a pure and perfect gas, and then he generalized his results for all ideal solutions. For component *i* in an ideal gas mixture he extracted the following relation

$$\mu_i - \mu_i^0 = k_B T \ln \frac{y_i p}{p^0} \quad (1.20)$$

where p is the pressure, p^0 a reference pressure usually taken as 1 bar, and y_i is the mole fraction of component i in the ideal gas mixture. Equation (1.20) indicates that, in an ideal gas mixture, the chemical potential μ_i of component i relative to the chemical potential μ_i^0 of component i in the pure ideal gas state at the reference pressure p^0 and at a temperature equal to the temperature of the mixture equals the product of $k_B T$ times the natural logarithm of the partial pressure $y_i p$ divided by the reference pressure. Eq. (1.20) establishes that the change in chemical potential of component i in an ideal gas mixture during an isothermal process can be replaced by $k_B T$ times the corresponding change in the natural logarithm of the partial pressure of i.

1.2.2 Ideal solutions

Ideal solutions are quite different from perfect gases, since the latter are not subject to any forces between molecules. In an ideal solution there are interactions between molecules of component 1 and component 2, although the average energy of 1-2 interactions is equal to the average energy of 1-1 and 2-2 interactions in the corresponding pure liquids at the same temperature and pressure.

Equation (1.20) can be applied only to perfect gaseous mixtures. In order to generalize it, Lewis defined a function for any component of any system undergoing an isothermal process that was named fugacity f through the equation

$$\mu_i - \mu_i^0 = k_B T \ln \frac{f_i}{f_i^0} \quad (1.21)$$

where either μ_i^0 or f_i^0 can be selected independently.

For a pure, perfect gas, fugacity is equal to pressure, while for a component *i* in a mixture of perfect gases, fugacity is equal to $y_i p$. Because of the fact that all systems tend to follow the behavior of perfect gas on low densities, the definition of that corrected pressure obeys the following rule

$$\text{for } p \to 0 : \frac{f_i}{y_i p} \to 1$$

where y_i is mole fraction of component *i*.

Thus, fugacity is a thermodynamic property with units of pressure that reexpresses the chemical potential. It is generally a function of temperature, pressure and composition and can be defined for every component i in a mixture through a differential equation and a boundary condition:

$$d\mu_i = k_B T \; d\ln f$$

$$\lim_{p\to 0} \frac{f_i}{y_i p} = 1$$

The latter definition makes it clear that the definition of fugacity is independent of the choice of a standard state.

Lewis named the fraction f_i / f_i^0 activity, a, since it provides an indication of how "active" a substance is, compared to the standard state. In general, the concept of fugacity leads from pure thermodynamics to the theory of intermolecular interactions. More specifically, if one considers fugacity as a corrected pressure, then these corrections are attributed to the non-ideality of intermolecular forces.

The condition of thermodynamic equilibrium between two phases, V and L (equality of chemical potentials between the phases for all components) can be translated into:

$$f_i^V = f_i^L \quad (1.22)$$

In the applications considered in this thesis, V will stand for the vapor phase and L for the liquid phase. At low pressures, the fugacity f_i^V of component i in the vapor phase under given pressure and temperature is proportional to the mole fraction y_i, meaning

$$f_i^V = y_i f_i^{V,\text{pure}} \quad (1.23)$$

where $f_i^{V,\text{pure}}$ is the fugacity of pure component *i* in the vapor phase, at the temperature and pressure of mixture. The exact same relation can be postulated for the liquid phase, where f_i^L is assumed proportional to the liquid mole fraction x_i as described in the following relation

$$f_i^L = x_i f_i^{L,\text{pure}} \quad (1.24)$$

where $f_i^{L,\text{pure}}$ is the fugacity of pure component *i* in the liquid phase, at the temperature and pressure of mixture. Equation (1.24), which is a generalization of Raoult's law, is known as Lewis's law or the Lewis and Randall rule. A liquid mixture satisfying eq (1.24) for all components *i* and for all compositions is an ideal solution.

Combining equations (1.22), (1.23) and (1.24) Lewis's law leads to

$$y_i f_i^{V,\text{pure}} = x_i f_i^{L,\text{pure}} \quad (1.25)$$

For a given temperature and low pressure, for a pure component *i* we know that $f_i^{V,\text{pure}} = p$. If the molar volume of pure liquid *i* is much smaller than the gaseous molar volume *RT*/*p* under the considered conditions, the pressure dependence of $f_i^{L,\text{pure}}$ can be neglected and its value set equal to the fugacity of pure saturated liquid *i* at the mixture temperature. From the vapor-liquid equilibrium condition of pure *i* at temperature *T* one then obtains

$$f_i^{L,\text{pure}} = p_i^s \quad (1.26)$$

where p_i^s is the saturated pressure of pure liquid *i* at the given temperature *T*.

Using (1.25), one can derive Raoult's law for an ideal solution at low pressure:

$$x_i p_i^s = y_i p \quad (1.27)$$

In order to replace the standard chemical potential μ_i^0, we apply eq. (1.20) for a system forming an ideal gas mixture in the vapor phase and an ideal solution in the liquid phase, and we subtract the equation of the gas from the one for the liquid. In this way we obtain

$$\mu_i^{\mathrm{id}} = \mu_{i,\mathrm{pure}} + k_{\mathrm{B}} T \ln x_i \quad (1.28)$$

where with μ_i^{id} we denote the chemical potential of I in an ideal solution.

An alternative way of describing ideal solutions is through activity coefficients. An ideal liquid solution is the one in which, under constant temperature and pressure, the activity for each component is proportional to mole fraction. The activity coefficient of a component *i* in a liquid solution is defined through the equation

$$f_i^L = \gamma_i f_i^0 x_i \quad (1.29)$$

where γ_i is the activity coefficient, f_i^0 is the fugacity of *i* at a reference state, known as standard sate, and x_i is the mole fraction of *i*. In any composition, γ_i depends on the selection of the standard state. The value of γ_i has no particular meaning,[17] unless the value of f_i^0 is initially defined. The activity coefficient is related to the activity according to relation

$$\gamma_i = \frac{a_i}{x_i} \quad (1.30)$$

For constant temperature and pressure we can write the following relation:

$$f_i^L = R_i x_i \quad (1.31)$$

where R_i generally depends on temperature, pressure, and composition, but becomes independent of composition when x_i is close to 1 or very small relative to 1. When x_i is very small relative to 1, then Henry's law is obeyed. In this case, R_i is Henry's constant H_i and it depends on temperature, pressure, and the mole fractions of the remaining components except *i*. When x_i is close to 1, Lewis's rule is obeyed and R_i is the fugacity of pure liquid *i* under the temperature and pressure of mixture. As seen from eq. (1.29), if $f_i^0 = R_i$, then $\gamma_i = 1$. If the relation $f_i^L = x_i f_i^0$ is obeyed for all components and for all compositions with f_i^0 being the fugacity of pure liquid *i* at the temperature and pressure of the mixture, then the solution is an ideal one, obeying Lewis's law. At low pressures, this reduces to Raoult's law, eq (1.29).

1.2.3 Real mixtures

Real binary mixtures consist of particles, for which interactions 1-1, 1-2, 2-2 are all different from one another. We now can adjust the expression (1.1) to take into account deviations from ideal behavior in real mixtures. Thus, in a real mixture the chemical potential is given by the following equation

$$\mu_i = \mu_i^0 + k_B T \ln(\gamma_i x_i) \quad (1.32)$$

Differentiation of the previous equation leads us to the following relation

$$x_i\left(\frac{\partial \ln \gamma_i}{\partial x_i}\right)_{T,P,x_{j\neq i},n} = \frac{x_i}{k_B T}\left(\frac{\partial \mu_i}{\partial x_i}\right)_{T,P,x_{j\neq i},n} - 1 \quad (1.33)$$

Once the derivative of chemical potential is calculated, a simple integration with respect to x_i allows the estimation of activity coefficients.

For a real mixture at low pressure we can also extend Raoult's law (1.27), using activity coefficients, to the following relation

$$\gamma_i x_i p_i^s = y_i p \quad (1.34)$$

1.3 Gibbs energy, enthalpy and entropy of mixing

In this section we consider the thermodynamics of mixing of liquids. First, we consider the simple case of liquids that mix to form an ideal solution. In this way, we identify the thermodynamic consequences of molecules of one species mingling randomly with molecules of the second species. The calculation provides a background for discussing the deviations from ideal behavior exhibited by real solutions [16].

The Gibbs energy of mixing for two liquids to form an ideal solution is calculated from relation

$$\Delta_{mix} G^{id} = k_B T(x_1 \ln x_1 + x_2 \ln x_2) \quad (1.35)$$

while entropy of mixing, multiplied by temperature, is given by

$$T\Delta_{mix} S^{id} = -k_B T(x_1 \ln x_1 + x_2 \ln x_2) \quad (1.36)$$

and, since $\Delta_{mix} H^{id} = \Delta_{mix} G^{id} + T\Delta_{mix} S^{id}$, the ideal enthalpy of mixing is zero. In ideal solutions there are interactions between molecules, but the average energy of 1-2 interactions in the mixture is the same as the average energy of 1-1, 2-2 interactions in the pure liquids.

Real solutions are composed of particles of which 1-1, 1-2, 2-2 interactions are all different. Not only may there be enthalpy and volume changes when liquids mix, but there may also be an additional contribution to the entropy arising from the way in which molecules of one type might

cluster together or be surrounded preferentially by molecules of another type (local composition), instead of mingling randomly with the others.

The thermodynamic properties of real solutions are expressed in terms of excess functions. An excess function is the difference between the observed thermodynamic function of mixing in the real solution and the corresponding function for an ideal solution of the same pressure, temperature, and composition. The Gibbs energy of mixing, for example, is defined as

$$\Delta_{\text{mix}}G = \Delta_{\text{mix}}G^{\text{id}} + G^{E} \quad (1.37)$$

The enthalpy of mixing can be directly calculated by the following relation

$$\Delta_{\text{mix}}H = H^{\text{mixture}} - x_1 H_1^{\text{pure}} - x_2 H_2^{\text{pure}} \quad (1.38)$$

where H^{mixture} is the enthalpy of the mixture, H_1^{pure} and H_2^{pure} are the enthalpies of pure components. The entropy of mixing, $\Delta_{\text{mix}}S$, and, more specifically, $T\Delta_{\text{mix}}S$, can be easily obtained by subtracting $\Delta_{\text{mix}}G$ from $\Delta_{\text{mix}}H$

$$T\Delta_{\text{mix}}S = \Delta_{\text{mix}}H - \Delta_{\text{mix}}G \quad (1.39)$$

Finally, one can easily transform these quantities to their corresponding molar quantities by multiplying them with the factor of N_{A}, as $\Delta_{\text{mix}}G_{\text{m}} = N_{\text{A}}\Delta_{\text{mix}}G$, $\Delta_{\text{mix}}H_{\text{m}} = N_{\text{A}}\Delta_{\text{mix}}H$, and $T\Delta_{\text{mix}}S_{\text{m}} = N_{\text{A}}T\Delta_{\text{mix}}S$.

1.4 Excess properties

Deviations of the excess energies from zero indicate the extent to which the solutions are nonideal. The thermodynamic properties of real solutions are expressed in terms of the excess

functions, X^{E}, i.e., differences between the observed thermodynamic function of mixing and the function of mixing for an ideal solution of the same temperature, pressure, and composition. The excess entropy, S^{E}, for example, is defined as

$$S^{E} = \Delta_{mix}S - \Delta_{mix}S^{id} \quad (1.40)$$

where $\Delta_{mix}S^{id}$ is given by eq. (1.36). The excess enthalpy is equal to the observed enthalpy of mixing, because the ideal value is zero. Considering excess enthalpy H^{E} qualitatively, if $H^{E} < 0$, then mixing is endothermic and the solute-solvent interactions are more favorable than the solvent-solvent and solute-solute interactions. If $H^{E} > 0$, then the mixing is endothermic. The excess Gibbs energy G^{E} is given from the above relation

$$G^{E} = \Delta_{mix}G - \Delta_{mix}G^{id} \quad (1.41)$$

For the calculation of G^{E} many methodologies have been developed and introduced over the years. One widely known, due to its simplicity, is the one originating in activity coefficients. It will be presented in Chapter 5. Another one, presented in Appendix 2, allows the extraction of G^{E} from the derivative of chemical potential with respect to composition through an iterative shooting method. Finally the relation linking all three excess quantities is the following:

$$TS^{E} = H^{E} - G^{E} \quad (1.42)$$

Chapter 2

2. Atomistic simulations

2.1 Introduction

Computational simulations reproduce the behavior of a system using a mathematical model. Simulations are used in many different scientific fields, from physics and chemistry to psychology and the social sciences. Using simulations, the behavior of a complicated system, dependent on many variables, can be reproduced, and therefore analyzed to extract significant properties and data. Computing simulations are, practically, programs executed for a short or long period of time.

Simulations link theory and experiment. For complicated systems that are difficult to handle in a laboratory, simulation may play the role of experiment. This is a common strategy, especially in materials simulations, where many limitations might exist on the laboratory environment. A theoretical model can be directly compared to simulation results. In case a theory based on a model does not come to agreement with simulation results of the same model, one can conclude that the theory is not sufficient for describing the system. In modern scientific work, a new theory is almost always accompanied by a simulation verifying it.

Using simulations, one can link a microscopic state to the microscopic nature of a given material. Simulations can also play a predominant role in building and analyzing a material's

structure, providing valuable insight on molecular configurations, physical and chemical properties. Inputs to the simulation are the geometry of molecules constituting the studied system, the force field assigned to describe interactions between atoms, and the macroscopic constraints applied on the system.

The main target of molecular simulations is the full thermodynamic analysis of a studied system. Although many thermodynamic properties can be easily extracted (density, enthalpy), molecular simulations do not provide a standard way for estimating "statistical" properties, such as entropy, chemical potential, or Gibbs energy of mixing. Various methodologies have been created and implemented over the years, in order to acquire such essential quantities.

By far the best known of these simulation techniques is the one proposed by B. Widom [4]. Widom based the extraction of all statistical thermodynamic properties on inserting a test particle that doesn't take part in system's evolution. Following this method's basic principles, certain particle deletion methods have been also proposed.[5,6] Unfortunately, methods based on particle insertion and deletion are not readily applicable to mixtures consisted of complicated molecules, such as the ones studied on this thesis. Randomly inserting large molecules will lead to overlaps with existing molecules, and consequently the energy change associated with the insertion will reach huge, practically infinite, values. For the exact same reason, insertion schemes are deficient under low temperature conditions as well. KB theory not only does not suffer from the limitations mentioned, but also offers an effective way of calculating properties such as the Gibbs energy of mixing.

2.2 Molecular Dynamics algorithm

The two basic simulation methods developed in the 1950's are Monte Carlo and Molecular Dynamics. The first one is a stochastic technique based on randomness, while the second one is based on calculation of quantities depending on time. In this thesis we have used the Molecular Dynamics technique, so we will elaborate on this only.

Molecular Dynamics (MD) is applicable in a wide range of scientific fields. It is based on numerical integration of Newton's equations of motion

$$m_i \frac{\mathrm{d}^2 \mathbf{r}_i}{\mathrm{d}t^2} = -\nabla \mathcal{V}(\{\mathbf{r}_j\}) \quad (2.1)$$

where m_i is the mass of particle i, $\mathbf{r}_i$ its position, and $\mathcal{V}(\{\mathbf{r}_j\})$ is the potential energy function, which depends only on the positions of all particles.

The key ingredient of MD simulations is the correct selection of $\mathcal{V}(\{\mathbf{r}_j\})$, which is commonly described by the term "force field." There are various strategies for force field development. On a small scale, detailed atomistic force fields are required to describe differences between atom types in the same environment.

The dynamical equations used in MD are not always Newton's equations of motion. Newton's equations maintain constant number of particles, volume and total energy, and as such lead to the microcanonical statistical ensemble, which in most cases is cumbersome to implemented, both in theory and in experiment. Equations of motion need to be altered so that they generate trajectories under constant temperature instead of constant energy, and/or constant pressure instead of

constant volume. This corresponds to Legendre transformations from the original microcanonical to the canonical (*NVT*) or isothermal-isobaric (*NpT*) ensemble.

There are different approaches to the integration of equations of motion. The integration of these equations is usually implemented using the well-known Verlet algorithm. This algorithm uses positions, velocities and accelerations at time t, and positions from the previous step, $\mathbf{r}(t-\delta t)$, for the calculation of new positions $\mathbf{r}(t+\delta t)$. Positions are expressed as

$$\begin{aligned}\mathbf{r}(\mathrm{t}+\delta t) &= \mathbf{r}(t)+\delta t\mathbf{u}(t)+\frac{1}{2}\delta t^2\mathbf{a}(t)+\ldots \\ \mathbf{r}(\mathrm{t}-\delta t) &= \mathbf{r}(t)-\delta t\mathbf{u}(t)+\frac{1}{2}\delta t^2\mathbf{a}(t)+\ldots\end{aligned} \quad (2.2)$$

where $\mathbf{u}(t)$ is velocity (first derivative of $\mathbf{r}(t)$), and $\mathbf{a}(t)$ is acceleration (second derivative of $\mathbf{r}(t)$ with respect to time). Adding equations (2.2) together we obtain

$$\mathbf{r}(\mathrm{t}+\delta t) = 2\mathbf{r}(t)-\mathbf{r}(\mathrm{t}-\delta t)+\delta t^2\mathbf{a}(t) \quad (2.3)$$

The velocity at time *t* now can be expressed using the following relation

$$\mathbf{u}(\mathrm{t}) = \frac{\mathbf{r}(\mathrm{t}+\delta t)-\mathbf{r}(\mathrm{t}-\delta t)}{2\delta t} \quad (2.4)$$

All Verlet algorithms have the advantage of providing an accuracy of $O(\delta t^4)$ on the positions and $O(\delta t^2)$ on the velocities and maintain time inversion symmetry.

2.3 Computer Clusters

A cluster is a combination of inter-connected computers working collaboratively, so that they can be considered as one united system. A computer cluster assigns the execution of a specific task to a node, which is controlled and programmed from the software.

The separate computers are inter-linked with one another through Local Area Networks (LAN), while each node executes its own distinct submitted task. In most cases, all nodes consisted of approximately identical hardware and run the same operating system (os), although in limited cases clusters made out of different hardware and running different os may be built.

Through clusters one can achieve high performance (fast execution of submitted tasks) when in need of high cpu power. Moreover, clusters have by far lower cost in comparison with individual machines with the same specifications. Consequently, clusters are extensively used for simulations of complicated systems such as polymers, or mixtures consisting of molecules with complex chemical constitution.

In this thesis we have performed MD simulations on clusters constructed from Dell processors (model name: Intel(R) Xeon(R) CPU E5645, cpu frequency: 2400.095 MHz, cache size: 12288 KB). More specifically, to conduct these simulations the clusters named Glass and Leonidas of the Computational Materials Science and Engineering Group (COMSE), have been used. Also, several simulations were carried out on the Dutch national e-infrastructure with the support of the URF Cooperative. In every simulation we have used nodes running on 16 cores processor, with 56GB of RAM.

Chapter 3

3. Systems studied

3.1 Simulation details

We have studied two sets of n-hexane/ethanol binary mixtures. The first set consists of 11 binary mixtures with mole fractions $x_1 = 0, 0.1, ..., 1$ ($x_1 = 0$ corresponds to pure ethanol, and $x_1 = 1$ corresponds to pure *n*-hexane) at *T*=298.15 K and *p*=1 atm, while the second one consists of 11 binary mixtures with the same mole fractions as the first set, at *T*=413.15 K and *p*=20 atm. The initial configurations for all mixtures were generated in cubic simulation boxes, under periodic boundary conditions, using the amorphous builder plug-in of the Materials and Process Simulation (MAPS) platform.[7] Each one of these mixtures consists of *N*=10,000 molecules. The force field assigned to our simulations is TRaPPE-UA; it will be analyzed in Section (3.2).

In order to examine system size effects that might affect the calculation of KB integrals, we have also generated two additional sets at *T*=298.15 K and *p*=1 atm, and *T*=413.15 K and *p*=20 atm, respectively. Each one of these mixtures consists of *N*=1,000 molecules.

For each mixture we performed MD simulations using the Large-Scale Atomic-Molecular Massively Parallel Simulator (LAMMPS) software[8] in the *NpT* ensemble. The total simulation time for all systems was 40 ns, of which the first 20 ns were considered as the equilibration stage. The integration step was 1 fs for all simulations and the cutoff radius of the Lennard-Jones potential

was set equal to $2.33\sigma_{max}$ (where σ_{max} is the maximum σ of all interaction sites) for all pairs. Ewald summation for Coulomb interactions has been replaced by the Particle-Particle Particle-Mesh Method (PPPM), as we found good agreement between them, and processing time was significantly lower for the PPPM. Analytical tail corrections to the Lennard-Jones interactions were applied based on the assumption of a uniform distribution of pairs beyond the cutoff radius.

Perhaps the most characteristic property of this studied mixture is its azeotropic behavior. A maximum on a pressure-composition phase diagram, such as the one presented in Fig. 1, may occur when the unfavorable interactions between *n*-hexane and ethanol increase the vapor pressure of the mixture far above the ideal value. In such cases G^E is positive (less favorable mixing than ideal), and there may be contributions to it from both enthalpy and entropy effects. Other examples exhibiting such azeotropic behavior include dioxane/water and ethanol/water.

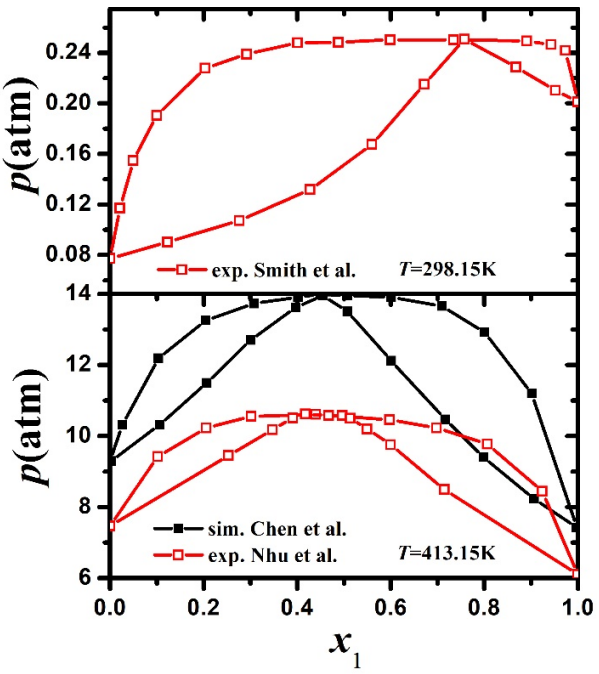

Fig. 1. Pressure composition diagrams for the binary mixtures of *n*-hexane/ethanol at *T*=298.15 K based on experimental data[11] (top), and for *T*=413.15 K based on simulation results[9] and experimental data[10] (bottom)

Deviations from ideality are not always so strong as to lead to a maximum or minimum in phase diagram, but when they are there are important consequences for distillation. Under the pressure and temperature at which the maximum is observed, the vapor and liquid phase that are in equilibrium with each other have the same composition. The mixture is said to form an azeotrope. When the azeotropic composition has been reached, distillation cannot separate the two components because the condensate has the same composition as the azeotropic liquid.

3.2 Force Field

The intramolecular and intermolecular interactions used in the description of a system are very important for the simulation performed. These interactions constitute the so-called force field. The total potential energy of the system, $\mathcal{V}$, is calculated as a sum of bonded and non-bonded interactions.

$$\mathcal{V}(\mathbf{r}_N) = \mathcal{V}_{\text{bonded}} + \mathcal{V}_{\text{non-bonded}} \quad (3.1)$$

where $\mathbf{r}_N$ is the vector of positions of all *N* atoms.

Interactions between atoms that are separated by more than three bonds, along a molecular chain, are described through a Lennard-Jones potential. Every united atom is represented by a spherical interaction center, the distance between centers *i* and *j* being denoted as r_{ij}

$$\mathcal{V}_{\mathrm{LJ}}(r_{ij}) = 4\varepsilon_{ij}\left(\left(\frac{\sigma_{ij}}{r_{ij}}\right)^{12} - \left(\frac{\sigma_{ij}}{r_{ij}}\right)^{6}\right) \quad (3.2)$$

where parameters ε and σ are given in Tables 1 and 2 of the Appendix 1. Parameters for pairs of unlike interaction sites are expressed in terms of parameters for pairs of like interaction sites using the Lorentz-Berthelot combining rules:

$$\begin{aligned} \varepsilon_{ij} &= (\varepsilon_{ii}\varepsilon_{jj})^{1/2} \\ \sigma_{ij} &= \frac{\sigma_{ii} + \sigma_{jj}}{2} \end{aligned} \quad (3.3)$$

Another non-bonded interaction is the Coulomb potential, which governs interactions between atomic charges, and is most commonly expressed as

$$U_{\mathrm{Coul}}(r_{ij}) = \frac{q_i\, q_j}{4\pi\varepsilon_0 r_{ij}} \quad (3.4)$$

where q_i and q_j are the charges on atoms *i* and *j*, respectively.

We also have three types of bonded interactions among the united atoms (pseudo-atoms)

$$\mathcal{V}_{\mathrm{bonded}} = \mathcal{V}_{\mathrm{bond}}(l) + \mathcal{V}_{\mathrm{bend}}(\theta) + \mathcal{V}_{\mathrm{torsion}}(\varphi) \quad (3.5)$$

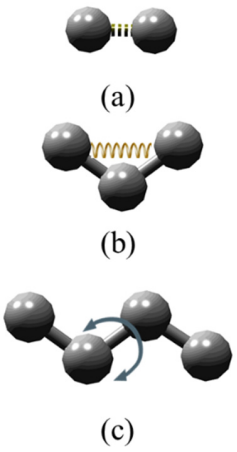

Fig. 2. Bonded interactions of (a) bond, (b) angle, and (c) dihedral angle

The bond stretching potential is considered as a harmomic one with large force constant. This implies high stiffness to the bonds, so that they cannot easily be stretched:

$$\mathcal{V}_{\text{bond}}(l) = \frac{1}{2} k_{\text{b}} (l - l_0)^2 \quad (3.6)$$

where l is the bond length, l_0 the bond length in the equilibrium state, and k_{b} the harmonic oscillator force constant. We also have a bond angle bending potential, involving angles formed between two consecutive bonds. This is, again, represented by a harmonic oscillator potential

$$\mathcal{V}_{\text{bend}}(\theta) = \frac{1}{2} k_{\theta} (\theta - \theta_0)^2 \quad (3.7)$$

where $(\pi - \theta)$ is the bond angle, and $(\pi - \theta_0)$ is the bond angle in the equilibrium state, while k_{θ} is the harmonic oscillator constant. Finally, the torsional potential is very important when it comes to distinguish *trans* from *gauche* configurations. This potential depends on the dihedral angle formed by four successive atoms along a molecular chain, or, equivalently, by three successive bonds. This is the dihedral angle between the plane defined by the first and second bonds and the plane defined by the second and third bonds.

$$\mathcal{V}_{\text{torsion}}(\varphi) = \sum_{n=1,5} A_{\text{n}} \cos^{n-1}(\varphi) \quad (3.8)$$

where φ is the torsional angle between two plains and A_{n}, n=1,2,...,5 are the constants of the dihedral potential. This torsion angle potential is in the multiharmonic style of Optimized Potentials for Liquid Simulations (OPLS). The *trans* state corresponds to $\varphi = \pi$. Potential parameters are given in Table 3 of Appendix 1.

Chapter 4

4. Methodology

4.1 Extension to Isobaric-Isothermal Ensemble

Our methodology is based on Kirkwood-Buff (KB) theory of solutions. As we described in section (3.1), simulations were performed in *NpT* ensemble in cubic simulation boxes under periodic boundary conditions. The definition of KB integrals given in eq. (1.1) can be extended to the *NpT* ensemble[12,13] using the relation

$$G_{ij}^{NpT} = \int_0^R [g_{ij}^{NpT}(r) - 1] 4\pi r^2 dr \quad (4.1)$$

where the upper limit of integration, R, delimits a region ($r < R$) within which the mixture composition differs from the overall composition of the bulk material.

On the other hand, in order to calculate KB integrals using the particle fluctuations method (pfm), based on equation (1.19), we first superimpose a three dimensional grid on our cubic simulation boxes. The simulation box is partitioned into smaller cells of edge length l_{cell} and volume V_{cell}. The smaller cells, capable of exchanging mass amongst them, follow the grand canonical ensemble. We define the parameter $\lambda = (V_{\text{cell}} / V_0)^{1/3}$, where V_0 is the minimum volume of the simulation box in the course of the *NpT* ensemble simulation. In the case of an *NVT* simulation, V_0 would be the constant volume of the simulation box.

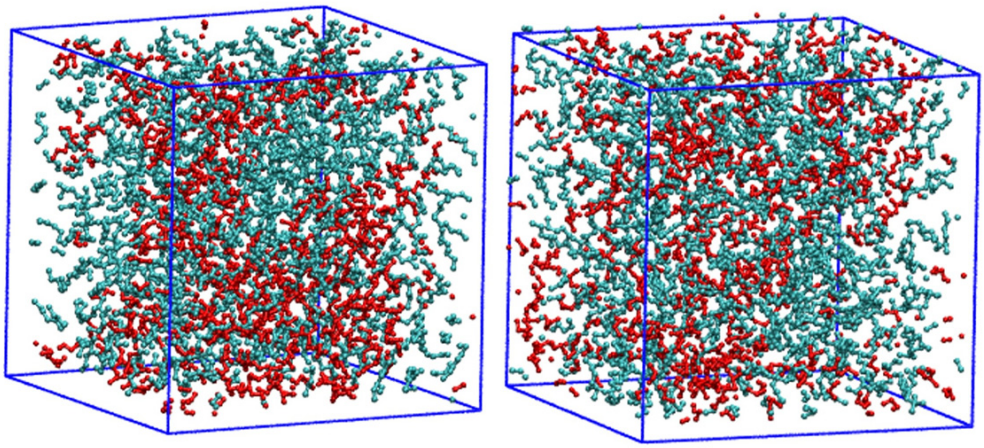

(a) *T*=298.15K, *p*=1atm **(b) *T*=413.15K, *p*=20atm**

Fig. 3. Snapshot of equimolar *n*-hexane/ethanol binary mixture at $T = 298.15\text{K},\ p = 1\text{atm}$ (a), as well as at $T = 413.15\text{K},\ p = 20\text{atm}$ (b). Cyan molecules represent *n*-hexane, while red molecules represent ethanol.

Then for each cell, *k*, we calculate the KB integrals $G_{ij,k}(\lambda)$ using equation (1.19). The average value over all N_{cells} cells is

$$G_{ij}(\lambda) = \frac{1}{N_{\text{cells}}} \sum_{k=1}^{N_{\text{cells}}} G_{ij,k}(\lambda) \quad (4.2)$$

for the current partitioning λ of the simulation box.

To calculate KB integrals in the thermodynamic limit from small sized MD simulations, we used the recently published work by Cortes-Huerto et al. [13] They introduced corrections firstly for the extension from the μVT ensemble, where KB theory was originally developed, to the NpT ensemble and secondly for periodic boundary conditions of a finite model system such as the ones

we study here. They finally extracted the following expression, which connects $G_{ij}(\lambda)$ KB integrals with G_{ij}^{∞}, which is the limiting value of G_{ij} at $V \to \infty$

$$\lambda G_{ij}(\lambda) = \lambda G_{ij}^{\infty}(1-\lambda^3) - \lambda^4 \frac{\delta_{ij}}{\rho_i} + \frac{\alpha_{ij}}{V_0^{1/3}} \quad (4.3)$$

where α_{ij} is a constant, which depends only on intensive thermodynamic system properties such as density and temperature, and ρ_i is the number density of species *i*.

4.2 Molecule and segment based methods

Having estimated G_{ij}^{∞}, one can proceed with the extraction of various thermodynamic properties applying the equations of KB theory. Ideal and real Lennard-Jones (LJ) binary mixtures have already been studied by Galata et al.[14] In our work we study *n*-hexane/ethanol binary mixtures, and to calculate particle fluctuations within the cells of the partitioned simulation box, we use two different methods.

In the **molecule based** method, we consider each molecule as a sphere (Fig. 4 (a), (b)) centered at its center of mass. In this way a particular molecule, as it evolves in the course of the MD trajectory, is transformed into a single interaction point, namely the position of its center of mass. This allows the extraction of fluctuations in the number of molecules from the exchange of these interaction points among cells of the partitioned simulation box.

In the **segment based** method, we divide each and every molecule into segments centered on specific (united) atoms of the molecule. Here a particular molecule is considered as a chain of segments, each segment representing a certain fraction of the molecule. The fraction assigned to

each segment is proportional to the molar mass of the atoms it comprises. As shown in Fig. 4 (c), (d), in this work each n-hexane molecule is viewed as an assemblage of six segments centered at the centers of its skeletal united atoms, whole each ethanol molecule is viewed as three segments, centered at the centers of its methyl group, its methylene group, and its oxygen atom. The hydrogen of the alcoholic –OH group is part of the third segment. The higher the molar mass of a segment [represented by a shadow in Fig. 4(c,d)], the larger the fraction of its molecule that it represents and the larger the contribution to fluctuations from this segment.

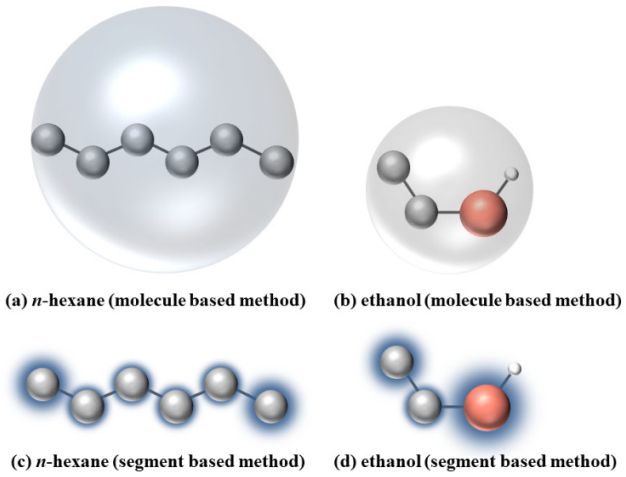

Fig. 4. Schematic presentation of molecule based method (a), (b), and segment based method (c), (d), used for calculating particle fluctuations

In Fig. 5 we plot $\lambda G_{ij}(\lambda)$ versus λ at T = 298.15 K, p=1 atm, and at T = 413.15 K, p=20 atm for a 10,000 molecule *n*-hexane/ethanol binary mixture of equimolar composition. We note that for lower λ values a linear behavior appears. This behavior is similar to the one observed in the works of Cortes-Huerto[13] and Galata et al. [14] In this linear regime we can fit a line whose slope, according to equation (5), is G_{ij}^{∞}.

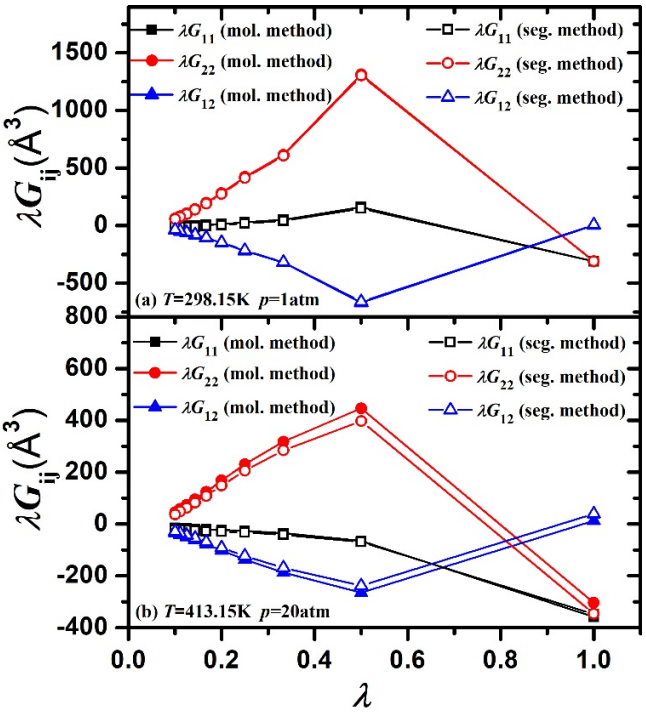

Fig. 5. Plot of λG_{11}, λG_{22}, λG_{12} versus λ for the equimolar n-hexane/ethanol binary mixture, at $T = 298.15\text{K}$, $p = 1\text{atm}$ (a), as well as at $T = 413.15\text{K}$, $p = 20\text{atm}$ (b), from both molecule and segment based methods

Chapter 5

5. Results and Discussion

In this section we present and discuss the results of our study of *n*-hexane/ethanol binary mixtures, using the particle fluctuation method, as proposed by Cortes-Huerto et al.[14] We post process our simulation trajectories using both the molecule and segment based methods outlined in Chapter 4 and we present pair distribution functions and KB integrals calculated from them as well as from the particle fluctuation method. We then calculate several thermodynamic properties, namely the activity coefficients of the two components relative to the pure liquids at the temperature and pressure of the mixture, the excess Gibbs energy, the excess enthalpy and the excess entropy as functions of composition. Note that in all figures error bars as obtained from averaging over multiple trajectories initiated at uncorrelated configurations, are very small, comparable to the size of the symbols, and therefore are omitted.

5.1 Density

One very important quantity that can be directly extracted from molecular dynamics simulation is the density of mixture. In Fig. 6 we plot the mass density ρ_{mass} versus the *n*-hexane mole fraction x_1. Results are shown for both the 1,000 and 10,000 molecule *n*-hexane/ethanol binary mixtures, which we simulated at both $T = 298.15$ K, p=1 atm and $T = 413.15$ K, p=20 atm. As expected, the densities of the big systems overlap with those of the small ones, and are independent of system

size. As x_1 increases, the density decreases monotonically, due to the appearance of more and more hydrogen bonds between ethanol molecules, which decreases the volume of the systems. Experimental data at $T = 298.15$ K and $p = 1$ atm [15] are in perfect agreement with our estimates.

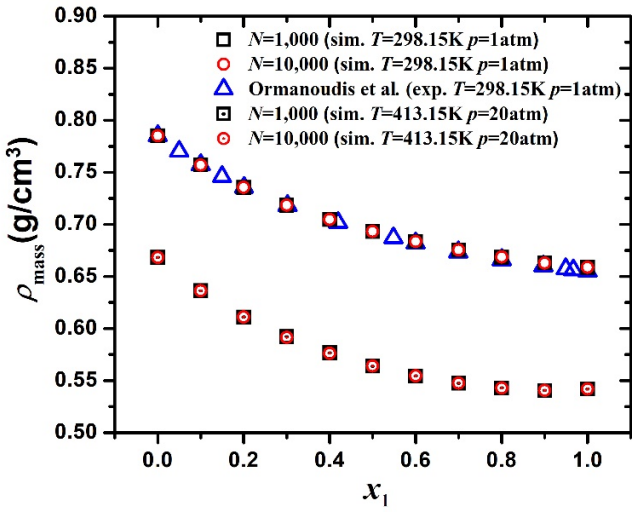

Fig. 6. Mass density of mixtures versus mole fraction of n-hexane for the n-hexane/ethanol binary mixture, simulated with 1,000 and 10,000 molecules at $T = 298.15\text{K},\ p = 1\text{atm},$ and at $T = 413.15\text{K},\ p = 20\text{atm},$ compared to experimental data at $T = 298.15\text{K},\ p = 1\text{atm}$ [15]

5.2 Pair distribution functions

KB integrals can be derived either from pair distribution functions, applying equation (4.1), or from particle fluctuations using the methodology by Cortes-Huerto et al., as described in the Methodology section. In order to calculate KB integrals using equation (4.1) we first need to calculate the pair distribution functions $g_{11}(r)$, $g_{12}(r)$ and $g_{22}(r)$.

In Fig. 7 we plot the three pair distribution functions between molecular centers of mass for mole fraction $x_1 = 0.5$ for both sets of conditions T=298.15 K, p=1 atm, and T=413.15 K, p=20

atm (calculated on 1,000 molecule systems, as pair distributions functions are not depended on system size). The distinguishably strong and sharp first peak (first neighbor) for $g_{22}(r)$ indicates that ethanol molecules tend to be in high proximity, since they form hydrogen bonds between them. Both $g_{11}(r)$ and $g_{12}(r)$ exhibit much flatter first peaks at higher distance (one has to reach a distance of at least 5Å before the first neighbor of *n*-hexane appears). One can easily observe that $g_{11}(r)$ practically does not form a second peak at all. On the contrary, both $g_{12}(r)$ and $g_{22}(r)$ form a second peak. This can be explained since in both $g_{12}(r)$ and $g_{22}(r)$ the first peak appears due to an ethanol molecule, while the second peak originates from the presence of a second ethanol hydrogen bonded to the initial one. For long distances $g_{11}(r)$, $g_{22}(r)$ and $g_{12}(r)$ tend to 1, which corresponds to the regime where there is no long-range order.

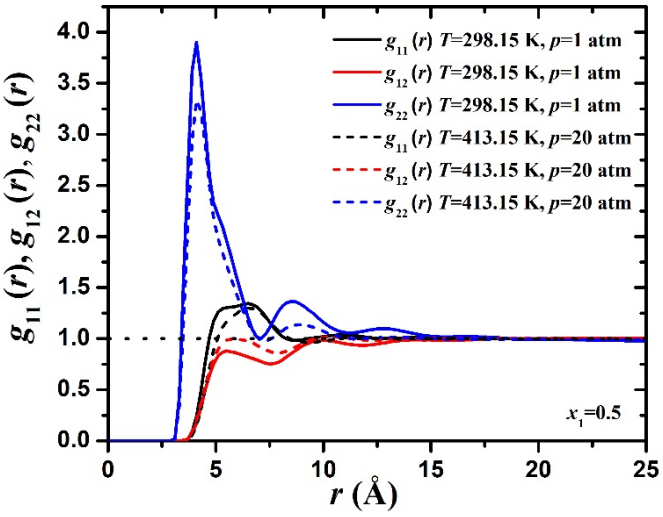

Fig. 7. Pair distribution functions for equimolar *n*-hexane/ethanol binary mixture versus distance *r,* for both $T = 298.15\text{K},\ p = 1\text{atm},$ and $T = 413.15\text{K},\ p = 20\text{atm}$

The numerical value of the pair distribution function $g_{22}(r)$ for *T*=413.15 K, *p*=20 atm is decreased in comparison to the one calculated for *T*=298.15 K, *p*=1 atm. This behavior can be

explained considering that, although hydrogen bonds are still formed in between ethanols at T=413.15 K, p=20 atm, as temperature increases, atoms tend to be way more active kinetically, and this inhibits the formation of strong intermolecular hydrogen bonds . The presence of a third peak in the T=298.15 K, p=1 atm system indicates that ethanol tends to form chains of hydrogen-bonded molecules up to the third neighbor, something not observed at T=413.15 K, p=20 atm.

5.3 Kirkwood-Buff integrals

Having calculated the pair distribution functions, we can easily estimate KB integrals $G_{11}(R)$, $G_{22}(R)$ and $G_{12}(R)$ from equation (4.1). In Fig. 8 we plot with black solid lines G_{11}, G_{22}, G_{12} against the distance R used as upper limit of integration for three different mole fractions $x_1 = 0.1, 0.5, 0.9$. For simplicity reasons we present results only for the T=413.15 K, p=20 atm system.

With red solid lines we plot the KB integrals for the smaller system, consisting of $N = 1,000$ molecules. We note that for the big system (N=10,000, black lines) KB integrals tend to a constant asymptotic value and are much better behaved than the ones from the small system. This significant distinction between the large and small systems clearly demonstrates how system size affects the KB integral calculation using pair distribution functions. For the small system (red lines) an asymptotic value is reached only for $G_{11}(R)$ when $x_1 = 0.9$ (excess of *n*-hexane), while $G_{22}(R)$ for $x_1 = 0.1$ (excess of ethanol) is also much better behaved than the rest of the pair distribution functions of the small system.

With dashed black and red lines we denote the estimates of G_{11}^{∞}, G_{22}^{∞}, and G_{12}^{∞} for the big and small system, respectively, using the fluctuation analysis and extrapolation procedure described in the Methodology chapter. We note that for most mole fractions, the two estimations deviate from each other, indicating that the particle fluctuation method is sensitive to system size as well. At the same time, the particle fluctuation method provides an acceptable estimation of KB integrals, while pair distribution functions totally fail to even converge on a constant value, especially for small systems. This is precisely the reason we chose to study our systems using the particle fluctuation method.

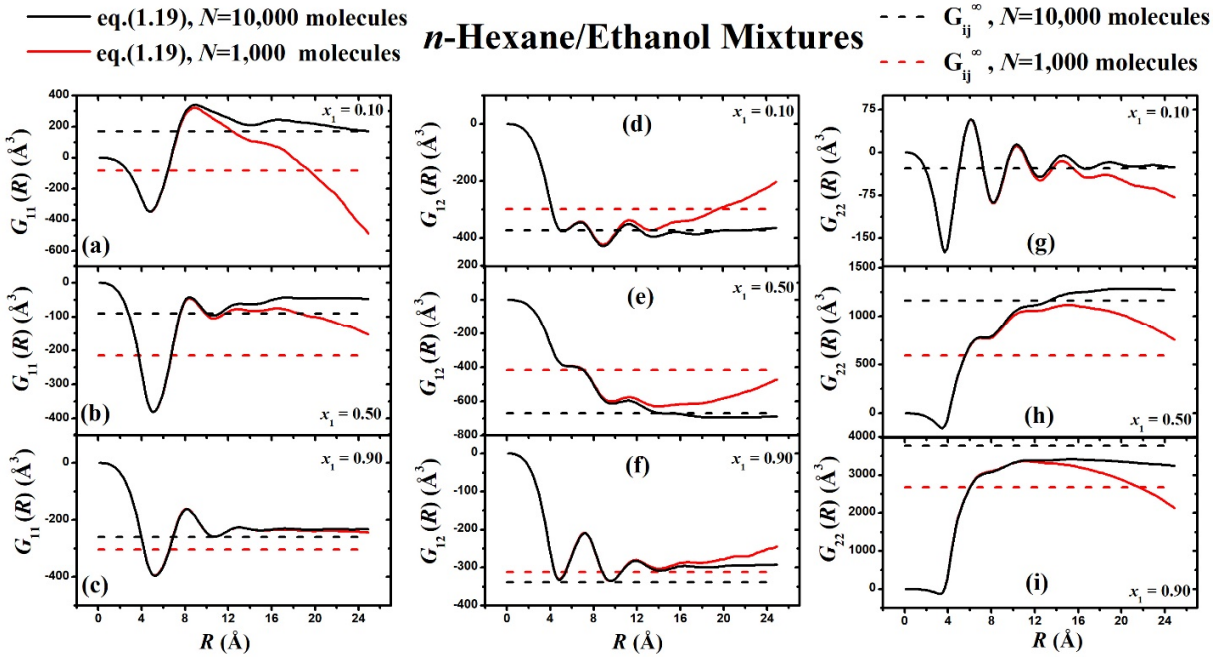

Fig. 8. KB integrals calculated from both pair distribution functions and particle fluctuations (calculated from molecule based method), for *n*-hexane/ethanol binary mixtures with *n*-hexane mole fractions $x_1 = 0.1, 0.5, 0.9,$ at T=413.15 K, p=20 atm.

Moreover, $G_{11}(R)$, $G_{22}(R)$ and $G_{12}(R)$ for long distances R in the big (10,000 molecule) systems tend to the G_{11}^{∞}, G_{22}^{∞}, and G_{12}^{∞} values, respectively, and thus the estimates of G_{11}^{∞}, G_{22}^{∞}, and G_{12}^{∞} using the Cortes-Huerto et al. particle fluctuation analysis - extrapolation methodology are validated. An even bigger system with $N > 10,000$ molecules would improve the estimation of G_{ij}^{∞}, and consequently of the thermodynamic properties of mixing and of the excess properties of the mixture.

5.4 Activity Coefficients

As already mentioned in section (1.3.2), activity coefficients are used in mixing thermodynamics to describe deviations from ideal mixtures. The derivative of the chemical potential on the r.h.s of eq. (1.33), the equation linking chemical potential to activity coefficient, can be calculated from the Kirkwood-Buff integrals using the following relation

$$\left(\frac{\partial \mu_1}{\partial x_1}\right)_{T,p} = \frac{k_B T \rho}{x_1\left[\rho_1 + \rho_2 + \rho_1\rho_2(G_{11}^{\infty} + G_{22}^{\infty} - 2G_{12}^{\infty}\right]} \quad (5.1)$$

where $\rho_1 = \frac{N_1}{\langle V \rangle}$ and $\rho_2 = \frac{N_2}{\langle V \rangle}$ are the number densities of components 1 and 2, respectively, $\langle V \rangle$ is the average volume of the NpT simulation, and $\rho = \rho_1 + \rho_2$.

Note that, as we have already described in the methodology chapter, the KB integrals G_{11}^{∞}, G_{22}^{∞} and G_{12}^{∞} are calculated for comparison by two methods, a molecule based method and a segment based method. Then, we can calculate activity coefficient of component 1, γ_1, by numerical

integration of equation (1.33) under the boundary condition $\gamma_1\left(x_1=1\right)=1$. The same procedure is followed for the second component (ethanol) and the calculation of activity coefficient γ_2.

In Fig. 9 we plot with black solid lines and black rectangles the activity coefficients γ_1 and γ_2 for the 1,000 molecule atomistic set of systems, as calculated using the molecule based method. Red solid lines and red circles depict activity coefficients again for the 1,000 molecule set of systems, as calculated using the segment based method. With olive (circles) and magenta (rectangles) colored lines, we plot activity coefficients from the 10,000 molecule systems using the molecule and segment based method, respectively. We notice that, for the same number of molecules, either 1,000 or 10,000, the estimates of the activity coefficients from both molecule based and segment based methods are within the error bars of the simulation, which are commensurate with the plotting symbol size. This is for both T=298.15 K, p=1 atm, and T=413.15 K, p=20 atm.

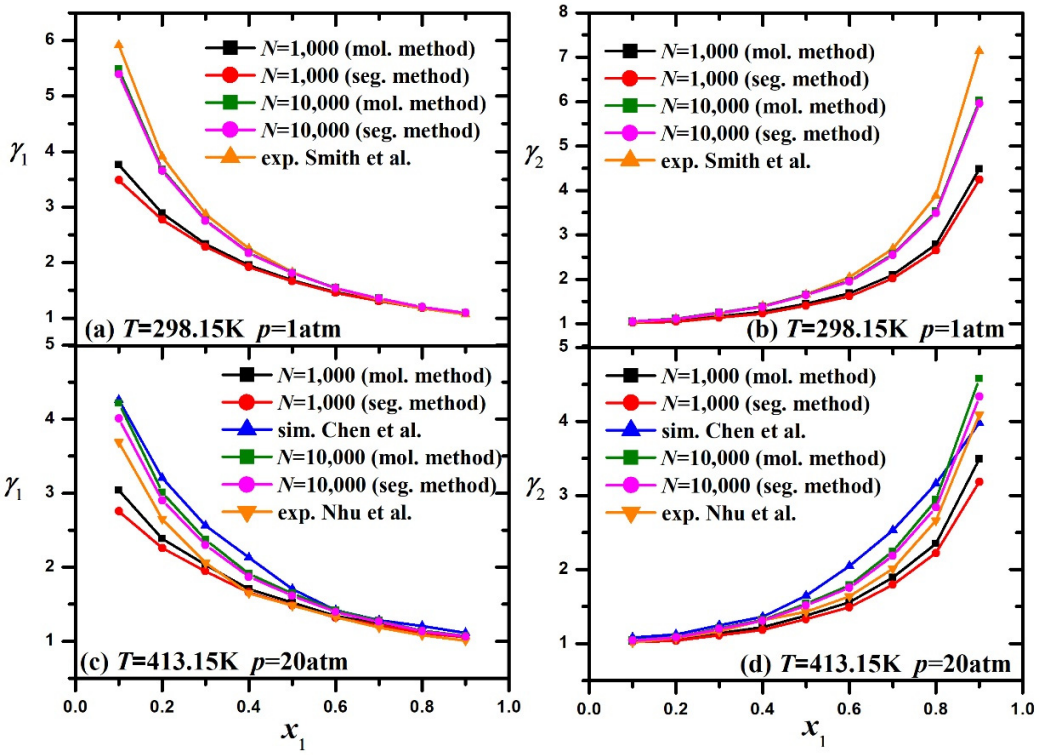

Fig. 9. Activity coefficients γ_1, γ_2 plotted versus *n*-hexane mole fraction x_1, for *n*-hexane/ethanol binary mixtures, as calculated from molecule based and segment based methods, being compared to experimental data at *T*=298.15 K, *p*=1 atm from Smith et al.[11] (a), (b). Activity coefficients γ_1 , γ_2 as calculated from molecule based and segment based methods being compared to values extracted from Chen's[9] simulations using the same force field and to experimental data from Nhu et al.[10] at *T*=413.15 K, *p*=20 atm (c), (d)

In order to validate our methodology and study how system size affects our results, we also extract activity coefficients γ_1 and γ_2 from the phase diagram $p(x_1, y_1)$ calculated from the Monte Carlo simulations of Chen et al's work,[9] as well as from experimental works. On this basis, we plot with blue solid lines and triangles the results from Chen et al.'s simulation, which was based

on the force field we employ here, while with orange lines and triangles experimental data from Nhu et al.[10] and Smith et al.[11] are depicted.

We note that both methods present strong system size effects; results from the 10,000 molecule simulations are much closer to the ones of Chen et al.'s simulation results and to experimental data. Any deviation between our simulation and Chen et al.'s simulation results could be explained considering that at pressure of 20 atm, fugacity coefficients for the pure liquid are not exactly equal to unity, and therefore the conversion of partial pressure to activity coefficients will suffer from small but considerable error in calculation. Both our simulation work and Chen et al.'s simulation results deviate from Nhu et al.s' experimental data, which is already justified from the disparity of Chen et al.'s simulation to experimental data in Figure 1(b). In the limit of $x_1 \to 1$ (infinite dilution of ethanol) $\gamma_1 \to 1$, while in the limit of $x_1 \to 0$ (infinite dilution of *n*-hexane) $\gamma_2 \to 1$. For all compositions both $\gamma_1 > 1$ and $\gamma_2 > 1$, indicating that the binary mixtures we study exhibit positive deviations from ideal solution behavior. The latter also indicates that *n*-hexane and ethanol molecules prefer to be surrounded by molecules of the same kind and thus their mixing is expected to be highly endothermic, as we will show in the next section. The main reason for this behavior is the formation of hydrogen bonds between ethanol molecules which amplify the attractive intermolecular same-species interactions.

5.5 Excess Gibbs Energy, excess enthalpy, and excess entropy

In this section we calculate the excess thermodynamic properties: excess enthalpy (H^{E}), excess Gibbs energy (G^{E}), and excess entropy (S^{E}) for the *n*-hexane-ethanol binary mixtures we

study. The excess enthalpy (H^{E}) is directly extracted from the simulations. The excess Gibbs energy (G^{E}) can be derived by two different methods. In the first we make use of the following differential equation

$$\left(\frac{\partial^2 \Delta_{\mathrm{mix}} G}{\partial x_1^2}\right)_{T,p} = \frac{1}{x_2}\left(\frac{\partial \mu_1}{\partial x_1}\right)_{T,p} = \frac{k_B T \rho}{x_1 x_2 \left[\rho_1 + \rho_2 + \rho_1 \rho_2 (G_{11}^{\infty} + G_{22}^{\infty} - 2G_{12}^{\infty})\right]} \quad (5.3)$$

under the boundary conditions $\Delta_{\mathrm{mix}} G(0) = 0$ and $\Delta_{\mathrm{mix}} G(0) = 1$. This is a second order boundary value problem. We solve the differential equation numerically using an iterative shooting method that it is outlined in Appendix 2. From that we obtain $\Delta_{\mathrm{mix}} G$ and then we easily derive G^E from (1.41). An alternative method for calculating G^E is through the activity coefficients, using the following relation

$$G^E = k_B T (x_1 \ln \gamma_1 + x_2 \ln \gamma_2) \quad (5.4)$$

In Fig. 9 we plot the molar excess Gibbs energy $G_{\mathrm{m}}^{\mathrm{E}} = N_{\mathrm{A}} G^{\mathrm{E}}$ versus the *n*-hexane mole fraction x_1, as derived using activity coefficients and the iterative shooting method for both sets of systems, at *T*=298.15 K, *p*=1 atm, and at *T*=413.15 K, *p*=20 atm. We present results from both 1,000 and 10,000 molecule MD simulations, as post processed using the molecule and segment based method. We also display the same quantities extracted from Chen's et al. [9] simulation results, and experimental data already mentioned in relation to activity coefficient figure. Note that symbols in Fig. 10 are the same as in Fig. 9.

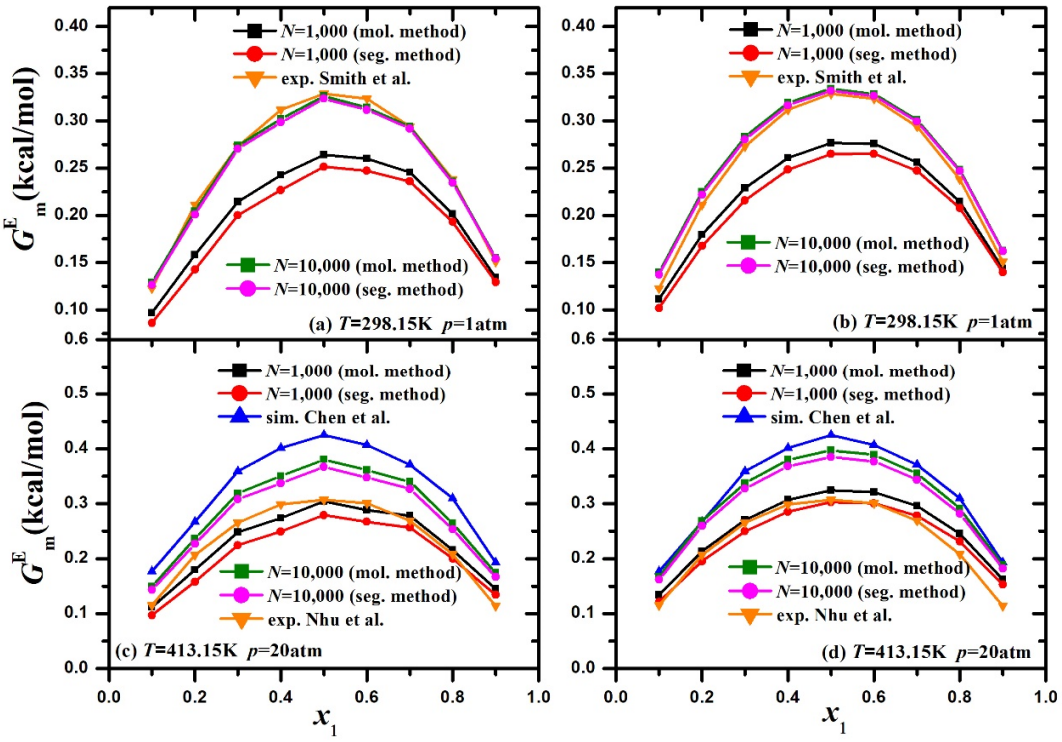

Fig. 10. Molar excess Gibbs energy plotted versus *n*-hexane mole fraction x_1, in *n*-hexane/ethanol binary mixtures, as calculated from molecule and segment based methods, using (a) the activity coefficients method based on eq. (5.3) and (b) the iterative shooting method based on eq. (5.2). Comparisons to experimental data collected at T=298.15 K, p=1 atm[11] are shown in parts (a) and (b) of the figure. Molar excess Gibbs energy also plotted for T=413.15 K ad p=20 atm, as calculated using (c) the activity coefficients method and (d) the iterative shooting method. In parts (c) and (d) comparisons are shown to Chen et al.'s[9] results based on the same force field and to experimental data [10] collected at T=413.15 K, p=20 atm.

As already shown on Fig. 9 there is a strong system size effect on both methods, since the 10,000 molecule MD simulation results are much closer to experimental data at T=298.15 K, p=1 atm, and to Chen's simulation results and to experimental data at T=413.15 K, p=20 atm, than the 1,000 molecule MD simulation results. Positive deviations from ideal mixture behavior are once again

observed, as in the activity coefficient results, Figure 9. The iterative shooting method forms a lot smoother curves than the ones derived using the activity coefficients method. Results from the iterative shooting method are also closer to Chen et al.'s simulation. With either method, a maximum is detected in the excess Gibbs energy of mixing at almost the same composition $x_1 = 0.5$. Post processing the 10,000 molecule simulation results using the molecule based method and the iterative shooting method describes our system in a more accurate way.

We now examine the excess molar Gibbs energy (G_m^E), excess molar enthalpy (H_m^E), and excess molar entropy (S_m^E) derived from our post process analysis**.** Since the iterative shooting method provides simulation estimates that are smoother and closer to experimental data, we will use G_m^E values based on this method for our analysis.

In Fig. 11 we plot with filled symbols the estimates from our MD simulations, while with open symbols we show results from various experimental and simulation works. Comparing simulation end experimental data for T=298.15 K, p=1 atm, for all three excess thermodynamic properties, we find very good agreement. The excess molar enthalpy H_m^E is positive, indicating that, as already anticipated in relation to the activity coefficients figure, the mixing process is highly endothermic. The excess molar entropy S_m^E at this temperature is negative, indicating that the entropy of mixing is lower than for an ideal solution. This can be explained, if one considers that chains of hydrogen bonded ethanol molecules are retained after mixing (see Figure 3a), leading to a rather ordered mixed state.

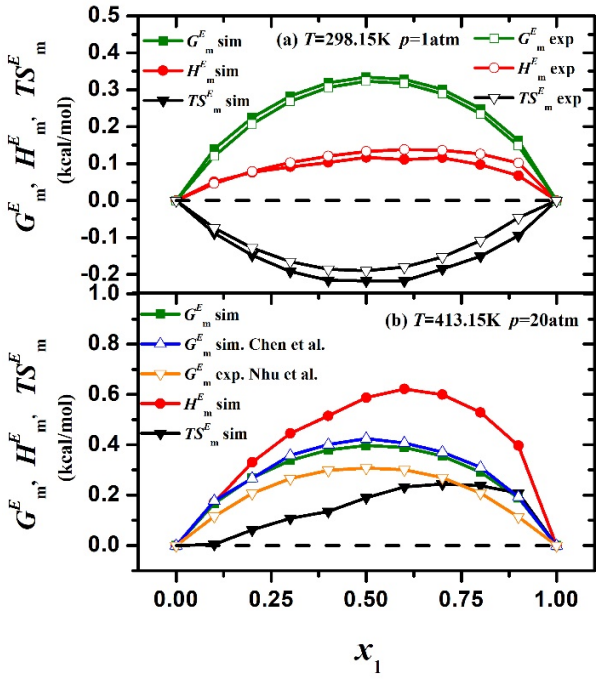

Fig. 11. Excess molar Gibbs energy, excess molar enthalpy, and excess molar entropy plotted versus *n*-hexane mole fraction x_1, for *n*-hexane/ethanol binary mixtures, and compared to experimental data at T=298.15 K, p=1 atm [11] (top). Excess molar Gibbs energy, excess molar enthalpy, and excess molar entropy plotted against x_1 and compared to Chen et al.'s simulation [9] (results extracted from phase diagram $p(x_1, y_1)$ generated on that work) and to experimental data at T=413.15 K, p=20 atm [10] (bottom).

On the contrary, one can easily observe that the H_m^E is very significantly increased at T=413.15 K, p=20 atm, forcing the excess molar entropy S_m^E (and consequently TS_m^E) to turn into positive quantities. This very interesting and unexpected change in the excess entropy of mixing at high temperature can be explained if one considers two opposing mechanisms. First, a thermal mixing of small and big molecules leads to negative deviations from ideal solution behavior (positive excess entropy of mixing), as pointed out long ago by Flory. [18] Secondly, hydrogen bonding brings

about local composition effects that reduce the entropy in relation to the random mixing characteristic of an ideal solution (negative excess entropy of mixing). The disparity in size between small ethanol molecules and big *n*-hexane molecules is moderate (see Figure 4). At low temperatures [T=298.15 K, p=1 atm system], where hydrogen bonding is strong, the second mechanism described above (local composition effects due to hydrogen bonding) wins and the excess entropy is negative (Figure 11, top). As temperature increases, hydrogen bonding gets less and less effective. Thus, at T=413.15 K, p=20 atm, hydrogen bonding in the mixture is weak and the second mechanism described above (disparity in size leading to nonrandom mixing) wins, leading to a positive excess entropy. Unfortunately, experimental data on the enthalpy of mixing are not available in the literature at T=413.15 K and p=20 atm to test this simulation prediction, although excess Gibbs energies are available through measurements of activity coefficients. It would be interesting to obtain enthalpy of mixing data experimentally and check if the predicted change in sign of $S_{\mathrm{m}}^{\mathrm{E}}$ with rising temperature and pressure is actually observed.

Conclusions

We have applied a general methodology to perform a full thermodynamic analysis of *n*-hexane/ethanol binary mixtures. The methodology is based on Kirkwood-Buff theory of solutions originally developed in the grand canonical, μVT, ensemble and extended to the isothermal-isobaric, NpT, ensemble as described in the work of Cortes-Huerto et al [13]. First, we compared the mass density derived from MD simulations with experimental data to validate the force field selected, obtaining excellent agreement.

We calculated pair distribution functions, extracting valuable insight into the structure and interactions present in the studied mixtures. Subsequently, KB integrals were calculated, using both particle fluctuation analysis and integration of the pair distribution functions. These calculations showed that the particle fluctuation method provides a more accurate estimation of KB integrals, especially when model systems of small size are used. A size of 10,000 molecules is deemed necessary for extracting reliable results via the KB approach. For the analysis of fluctuations in the number of molecules within cells embedded in the simulated model systems we have developed both a molecule-based strategy, considering only molecular centers of mass, and a segment-based strategy, considering centers of molecular fragments as representative of fractional molecules. Both strategies led to identical results, the segment-based strategy being more expensive computationally but subject to less statistical error. We estimated activity coefficients (γ_1 and γ_2), excess molar Gibbs energy (G^E), and we found good agreement with experimental data and Chen et al.'s previous simulations using the same force field. We also

calculated the excess molar enthalpy (H_m^E), and excess molar entropy (S_m^E) as functions of composition. We showed that the excess Gibbs energy is positive (positive deviations from ideal solution behavior) and that the excess molar enthalpy is positive (endothermic mixing) under all conditions studied. Experimental data for G_m^E and H_m^E, where available, fully confirm our simulation predictions. An interesting result from the simulations, which has not yet been explored experimentally, is that the excess entropy of mixing S_m^E switches from negative to positive as temperature and pressure rise from T=298.15 K and p=1 atm to T=413.15 K and p=20 atm. This peculiar behavior could be explained by considering two opposing tendencies: (a) hydrogen bonding of ethanol molecules in the mixture, the resulting chains of hydrogen-bonded molecules causing the mixture molar entropy to be lower than would be the case for random mixing at the molecular level; (b) the size difference between ethanol and n-heptane, causing the molar entropy of mixing to be higher than for a mixture of molecules of identical sizes and interactions. Based on our analysis, Kirkwood-Buff theory, and especially the extrapolation proposed by Cortes-Huerto et al. [13] to deal with finite system size and cell size in the analysis of particle number fluctuations, provides an efficient and accurate methodology for a full thermodynamic analysis, even for mixtures consisting of molecules with complicated shapes and interactions. On this basis, polymer blends can also be analyzed using the proposed methodology.

Future Work

In this thesis we have developed a general methodology for calculating thermodynamic properties of mixtures which consist of molecules with complex chemical constitution. Upcoming work could extend the current methodology to oligomeric blends. In such complex mixtures, classical molecule insertion or deletion schemes are not likely to succeed. Using Kirkwood-Buff theory, on the other hand, one can estimate the excess Gibbs energy, and consequently the Gibbs energy of mixing, in a most efficient and acceptable way, within a controllable margin of error. The only prerequisite is that systems of sufficient size be simulated. Using the methodology adopted on this thesis, KB integrals can be easily calculated from atomistic simulations of a real mixture simulated in the isothermal-isobaric ensemble. Through these KB integrals thermodynamic properties of mixing, and excess properties can be directly derived.

Appendix 1

Force field parameters of the molecular model TraPPE-UA, used in this thesis, are provided by Chen et al. [8] and listed in the following tables.

Interaction site	σ [Å]	ε [kcal mol^{-1}]	q[e]
CH_2	3.95	0.0914	0.0
CH_3	3.75	0.195	0.0

Table 1: Lennard – Jones potential parameters of TraPPE-UA for *n*-hexane

Interaction site	σ [Å]	ε [kcal mol^{-1}]	q[e]
CH_2	3.95	0.0914	0.0
CH_3	3.75	0.195	0.265
O	3.02	0.185	-0.7
H	0.0	0.0	0.435

Table 2: Lennard – Jones potential parameters of TraPPE-UA for ethanol

Bond stretching parameters	l_0 [Å]	k_B [kcal mol^{-1} Å^{-2}]
CH_x – CH_y	1.54	500.00
CH_2 – OH	1.43	500.00
H – OH	0.945	500.00
Angle bending parameters	**$\pi - \theta_0$ [deg]**	**k_θ [kcal mol^{-1}deg^{-2}]**
CH_3 – CH_2 – OH	109.5	50.077
CH_x – CH_2 – CH_y	114.00	62
CH_2 – OH – H	108.5	55.045

Dihedral parameters	A_1 [kcal mol^{-1}]	A_2 [kcal mol^{-1}]	A_3 [kcal mol^{-1}]	A_4 [kcal mol^{-1}]	A_5 [kcal mol^{-1}]
CH_x–CH_2–OH–H	0.674	0.703	0.115	-1.493	0.000
CH_x–CH_2–CH_2–CH_y	2.006	4.011	0.271	-6.288	0.000

Table 3: Bonded interaction parameters

Appendix 2

In order to solve the differential equation (5.1) numerically, we use an iterative shooting method. In particular, beginning with an initial guess for the first derivative of the Gibbs energy of mixing (which actually represents the slope of our curve), $\frac{\partial \Delta_{mix} G}{\partial x_1}(0)$, and knowing from the first boundary condition that $\Delta_{mix} G(0) = 0$, we can obtain, using forward first order finite differences:

$$\Delta_{mix} G(0.05) = \Delta_{mix} G(0) + 0.05 \frac{\partial \Delta_{mix} G}{\partial x_1}(0)$$

Then, we can invoke the recursive relation

$$\Delta_{mix} G(x_1 + h) = h^2 \frac{\partial^2 \Delta_{mix} G}{\partial x_1^2}(x_1) + 2\Delta_{mix} G(x_1) - \Delta_{mix} G(x_1 - h)$$

where $h = \Delta x_1 = 0.05$ is the mole fraction 'step' of our simulations and extract the function $\Delta_{mix} G(x_1)$ for all $x_1 \in [0, 1]$. If the estimated $\Delta_{mix} G(1)$ is not close to zero (second boundary condition), within a given tolerance, a new corrected value for $\frac{\partial \Delta_{mix} G}{\partial x_1}(0)$ is selected, via a

Newton-Raphson method, and the procedure is repeated. In Fig. 12 we show a flow diagram of the iterative shooting method we described above.

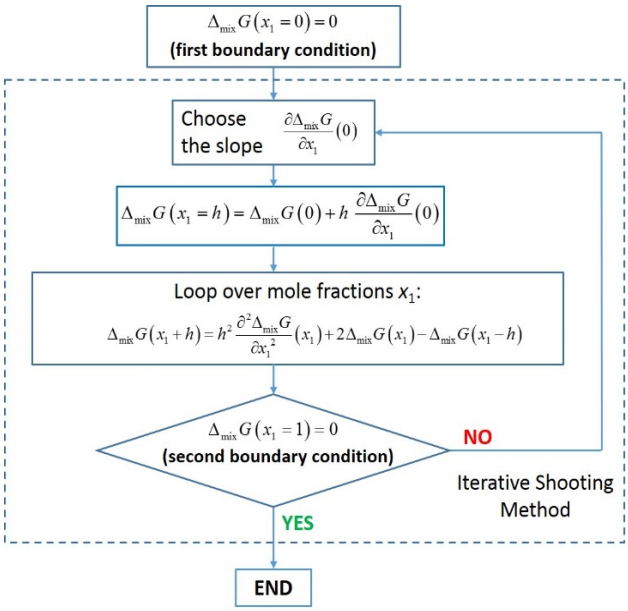

Fig. 12. Flow diagram of the iterative shooting method we apply to numerically solve equation (5.1)

Bibliography

(1) Kirkwood J.G.; Buff F.P.; The statistical mechanical theory of solutions, *J. Chem. Phys*. **1951**, *19*, 774-777.

(2) Ben-Naim A.; A Critique of Some Recent Suggestions to Correct the Kirkwood-Buff Integrals, *J. Phys. Chem. B*. **2007**, *111*, 2896-2902.

(3) Ben□Naim A.; Inversion of the Kirkwood–Buff theory of solutions: Application to the water–ethanol system, *J. Chem Phys.* **1977**, *67*, 4884-4890.

(4) Widom B.; Some topics in the theory of fluids, *J. Chem. Phys*. **1963**, *39*, 2808.

(5) Boulougouris G.C.; Calculation of the Chemical Potential beyond the First-Order Free-Energy Perturbation: From Deletion to Reinsertion, *J. Chem. Eng. Data*. **2010**, *55*, 4140–4146.

(6) Boulougouris G.C.; Economou I.G.; Theodorou D.N.; On the Calculation of the Chemical Potential Using the Particle Deletion Scheme, *Mol. Phys*. **1999**, *96*, 905–913.

(7) ‘‘http://scienomics.com/,’’ [Online].

(8) “http://lammps.sandia.gov,” [Online].

(9) Chen B.; Potoff J. J.; Siepmann J. I. Monte Carlo Calculations for Alcohols and Their Mixtures with Alkanes. Transferable Potentials for Phase Equilibria. 5. United-Atom Description of Primary, Secondary, and Tertiary Alcohols, *J. Phys. Chem. B.* **2001**, *105*, 3093-3104.

(10) Nhu N. V.; Liu A.; Sauermann P.; Kohler F.;. On the thermodynamics of ethanol + hexane at elevated temperatures and pressures, *Fluid Phase Equilib.* **1999**, *145*, 269-285.

(11) Smith V. C.; Robinson L. R.; Vapor-Liquid equilibria at 25C in the binary mixtures form by hexane, benzene, and ethanol, *J. Chem. Eng. Data.* **1970**, *15*, 3-395

(12) Krüger P.; Schnell S.K.; Bedeaux D.; Kjelstrup S.; Vlugt T.J.H.; Simon J.-M.; Kirkwood−Buff Integrals for Finite Volumes, *J. Phys. Chem. Lett*. **2013**, *4*, 235−238.

(13) Cortes-Huerto R.; Kremer K.; Potestio R.; Kirkwood-Buff integrals in the thermodynamic limit from small-sized molecular dynamics simulations, *J. Chem. Phys*. **2016**, *145*, 141103.

(14) Galata A.A.; Anogiannakis S.D.; Theodorou D.N.; Thermodynamic Analysis of Lennard-Jones binary mixtures using Kirkwood-Buff theory, *Fluid Phase Equilib.* **2018**, *470*, 25-27.

(15) Ormanoudis C.; Dakos C.; Panayiotou C.; Volumetric Properties of Binary Mixtures 2. Mixtures of *n*-Hexane with Ethanol and 1-Propanol, *J. Chem. Data.* **1991**, *36*, 39-42.

(16) Atkins P.; and Paula J.; Physical Chemistry, 8th ed, *Oxford Univ. Press*. **2006**, pp. 79.

(17) Haase R.; Physical Chemistry, An Advanced Treatise, *Academic Press N.Y*. **1971**, pp. 24-28

(18) Flory P. J. Principles Of Polymer Chemistry, *Cornell University Press*. **1953**